Spectroscopic- and Computational Insight into the Activation of O_2 by the Mono-nuclear Cu Center in Polysaccharide Monooxygenases

Christian H. Kjaergaard[a], Munzarin F. Qayyum[a], Shaun D. Wong[a], Feng Xu[b], Glyn R. Hemsworth[c], Daniel J. Walton[c], Nigel A. Young[d], Gideon J. Davies[c], Paul H. Walton[c], Katja S. Johansen[e], Keith O. Hodgson[a,f], Britt Hedman[f], and Edward I. Solomon[a,f,1]

[a]Department of Chemistry, Stanford University, Stanford, CA 94305; [b]Novozymes, Inc., Davis, CA 95618; [c]Department of Chemistry, University of York, Heslington, York YO10 5DD, United Kingdom; [d]Department of Chemistry, University of Hull, Kingston upon Hull HU6 7RX, United Kingdom, [e]Novozymes A/S, DK-2880, Bagsværd, Denmark; and [f]Stanford Synchrotron Radiation Lightsource, SLAC, Stanford University, Stanford, CA 94309

[1]To whom correspondence may be addressed. E-mail: Edward.solomon@stanford.edu

Author contributions: C.H.K. and E.I.S. designed research; C.H.K., M.F.Q., and S.D.W performed research; F.X. expressed and purified enzyme; C.H.K. and E.I.S. wrote the manuscript. C.H.K., M.F.Q., S.D.W., F.X., G.R.H., D.J.W., N.A.Y., G.J.D., P.H.W., K.S.J., K.O.H., B.H., and E.I.S. analyzed data.

Conflict of interest statement: F.X. and K.S.J. are employees of Novozymes, which is a major enzyme producing company.

Abstract

Strategies for O_2 activation by copper enzymes were recently expanded to include mononuclear Cu sites, with the discovery of the copper-dependent *polysaccharide monooxygenases*, also classified as auxiliary-activity enzymes 9-11 (AA9-11). These enzymes are finding considerable use in industrial biofuel production. Crystal structures of PMOs have emerged, but experimental studies are yet to determine the solution structure of the Cu site and how this relates to reactivity. From XANES and EXAFS spectroscopies, we observed a change from 4-coordinate Cu(II) to 3-coordinate Cu(I) of the active site in solution, where three protein-derived nitrogen ligands coordinate the Cu in both redox states, and a labile hydroxide ligand is lost upon reduction. The spectroscopic data allowed for Density Functional Theory calculations of an enzyme active site model, where the optimized Cu(I) and (II) structures were consistent with the experimental data. The O_2 reactivity of the Cu(I) site was probed by EPR and stopped-flow absorption spectroscopies, and a rapid one-electron reduction of O_2 and regeneration of the resting Cu(II) enzyme were observed. This reactivity was evaluated computationally, and by calibration to Cu-superoxide model complexes, formation of an end-on Cu-AA9-superoxide species was found to be thermodynamically favored. We discuss how this thermodynamically difficult one-electron reduction of O_2 is enabled by the unique protein structure where two nitrogen ligands from His1 dictate formation of a T-shaped Cu(I) site, which provides an open coordination position for strong O_2 binding with very little reorganization energy.

Significance

Activation of the O-O bond in dioxygen is difficult but fundamental in biology. Nature has evolved several strategies to achieve this, often including copper as an enzyme co-factor. Copper-dependent enzymes usually employ more than one metal to activate O_2 by multi-electron reduction, but recently it was discovered that cellulose and chitin degrading *polysaccharide monooxygenase* enzymes utilize only a single Cu center for catalysis, in a reaction that is of great interest to the biofuel industries. To understand this reactivity, we have determined the solution structures of both the reduced and oxidized Cu site, and determined experimentally and computationally how this site is capable of facile O_2 activation by a thermodynamically difficult one electron reduction, via an inner-sphere Cu-superoxide intermediate.

1. Introduction

Cu is an important metal-cofactor in a number of enzymes that activate dioxygen for reactivity. Several classes with either bi- or trinuclear copper active sites have been identified and their different strategies for O_2 activation have been elucidated (1). These include the multicopper oxidases that utilize three Cu ions to reduce O_2 to water with very little overpotential (2, 3), the coupled binuclear Cu enzymes that are involved in dioxygen transport and monooxygenase reactivity (4), and the non-coupled binuclear Cu monooxygenases that activate O_2 for hydroxylation of peptides and hormones (5). Recently, a new class of oxygen activating enzymes with a single copper center has been identified, the *Polysaccharride Monooxygenases* (PMOs) (6-8), or AA9 to 11 enzymes (AA = auxiliary activity) in the CAZY database (9). AA9 enzymes (formerly Glycoside Hydrolases family 61 (GH61s)) are fungal enzymes that can enhance major cellulases' enzymatic degradation of cellulose (hence "auxiliary activity"), whereas AA10 enzymes (formerly Carbohydrate Binding Module family 33 (CBM33)) are predominantly bacterial enzymes that can enhance major chitinases' degradation of chitin (6,7,10-13). Enzymes in the latest discovered subclass, AA11, are fungal enzymes, where the currently lone characterized example utilizes chitin as a substrate (8). Studies by Vaaje-Kolstad et al. (6) and Beeson et al. (14) have shown that AA10 and AA9 introduce a single oxygen atom originating from dioxygen into the respective chitin and cellulose degradation products. Although little is known about the reaction mechanism of these enzymes, it is believed that this does not simply involve Fenton type chemistry producing reactive oxygen species, but rather a more controlled reaction involving a Cu-oxygen intermediate (14-16). Cu-loaded crystal structures have been solved for all three

subclasses of AA9-11 enzymes (7, 8, 17-19), highlighting interesting similarities and differences. Common for the three classes is a flat protein surface that harbors the Cu active site, as illustrated for an AA9 enzyme in Fig. 1, left. In AA9 PMOs, the flat surface is proposed to interact with the long-chained substrates via a number of primarily aromatic amino acids (18,19). In the active Cu site, two histidines provide three nitrogen ligands, two from N-His and one from the terminal amine (Fig. 1, right), in a configuration that has been termed a histidine brace (7). An axially oriented tyrosine is highly conserved in the AA9 and AA11 enzymes ~3Å from the Cu, and hydrogen bonded to an oxygen from a glutamine or glutamate side chain (see Fig. 1, right). In the AA10 enzymes, the axial Tyr is replaced with a highly conserved phenylalanine. In addition to these amino acids, water derived molecules are often refined in the vicinity of the Cu ion, but it is not known whether these coordinate to the Cu in solution. Although the crystal structures provide valuable information, they do not determine the detailed environment of the Cu ion in solution, which is critical in elucidating the mechanistic properties of the PMOs. This is partly due to the fact that oxidized Cu readily undergoes photoreduction upon exposure to X-rays, often accompanied by changes in the coordination environment of the metal (20).

The PMO superfamily is of considerable importance in the developing area of 2nd generation (recalcitrant polysaccharide) biofuels, where even preliminary studies have shown 2-6 fold improvements in biomass conversion using unoptimized mixtures (6,11) providing further impetus for their detailed characterization. Here we present spectroscopic results on a PMO from *Thermoascus aurantiacus*, denoted Cu-AA9, complimented by Density Functional Theory (DFT) calculations that provide a detailed

description of the coordination environment in solution of both the oxidized and reduced Cu active site. Furthermore, the interaction of the reduced Cu site with dioxygen is investigated, focusing on the ability of the PMOs to activate O_2 with a single Cu center.

2. Results and Analysis

2.1 Cu K-edge XANES and EXAFS

2.1.1 Oxidized and reduced Cu-AA9

Cu K-edge XANES spectra of reduced and oxidized Cu-AA9 are shown in Fig. 2. In the first fast scan of Cu(II)-AA9 (blue trace) (radiation dose: ~$1.7x10^{12}$ photons/mm^2), very little intensity at 8984eV is seen, verifying the presence of the oxidized state of the Cu. However, the oxidized enzyme undergoes photoreduction in the beam as observed in the average of longer scans from four fresh spots (black dashed trace) (radiation dose: ~$6.6x10^{12}$ photons/mm^2 per scan), similar to observations for AA10 PMOs (17). In contrast, the spectrum of the fully reduced state (red trace, Fig. 2) does not change with time (i.e. no further photoreduction) and has an intense 8984eV feature with normalized intensity of 0.76 originating from a Cu 1s to 4p transition (21). The intensity and shape of the rising edge in the Cu(I) XANES spectrum is consistent with a 3-coordinate (either three equidistant ligands or two short plus one longer distance ligands (i.e. T-shaped)) Cu(I) based on results from previously studied model Cu(I) complexes (22).

EXAFS was performed on the oxidized and reduced enzyme forms to determine the number and type of coordinating ligands to the Cu ion in Cu-AA9. As seen in Figs. 3A and B, the beat-pattern and the Fourier transform of the Cu(II) enzyme can be simulated with a first sphere of four O/N ligands at an average distance to the Cu(II) ion of 1.98Å (Table 1A). Alternatively, the reduced enzyme requires two ligand sets to fit the first coordination sphere and is simulated with three first-sphere O/N ligands, two at 1.90Å and one at 2.25Å (Figs. 3C and D and Table 1B). This reveals that upon reduction in solution, the AA9 enzyme changes from a four-coordinate Cu(II) to a three-coordinate

T-shaped Cu(I) site structure. We note that the beat pattern and Fourier transform of Cu(II)-AA9 closely resembles that of the oxidized form of copper *particulate methane monooxygenase* (pMMO) (23,24), the only other Cu enzyme known to employ the histidine brace (6,19). In contrast to Cu-pMMO, however, the simulation for Cu(II)-AA9 does not require a second Cu ion to be included in the set of nearby scattering atoms.

2.1.2 Cryo-reduction of Cu(II)-AA9.

To probe the temperature dependence of the reduction-induced change in the coordination environment of Cu-AA9, cryo-reduction (at 77K) of Cu(II)-AA9, followed by XANES and EXAFS evaluation, was performed. A Cu(II)-AA9 sample was prepared in a cryo-cell, frozen in liquid nitrogen, and subsequently exposed to a γ-emitting ^{137}Cs source that produces free electrons in the cryo-solvent. The extent of cryo-reduction of Cu(II)-AA9 was monitored by the disappearance of the characteristic Cu(II)-AA9 EPR spectrum (7) (Fig S2). After 110 hours of exposure time (~5.9Mrad total dose), the enzyme was ~75% reduced. The XANES spectrum of the ~75% reduced Cu-AA9 (Fig. 4, green trace) has a prominent 8984eV feature that further increases by exposure to the synchrotron beam with the final spectrum (black trace) estimated to be ~90% reduced, as compared to the solution reduced enzyme (red trace, from Fig. 2). The shape of the rising edge in the ~90% cryo-reduced sample is similar to that of the solution-reduced peak. Further, the EXAFS data and simulation (Fig. S3, Table S1) of the cryo-reduced Cu-AA9 sample are consistent with a mixture of the oxidized and reduced forms, with the reduced form dominant. Therefore, the observed change in coordination environment of the Cu-ion upon reduction at room temperature, from four-coordinate to three-coordinate, also

occurs in the frozen enzyme at 77K. The fact that this geometry change also occurs at low temperature is indicative of limited rearrangement in the protein structure, consistent with the three protein-derived nitrogen ligands identified in crystal structures (2xN-His, 1xN-terminal amine, see Fig. 1) coordinating the Cu in both the reduced and oxidized state, whereas the water derived ligand is labile and only coordinates to the oxidized Cu center.

2.2 Reactivity of reduced Cu(I)-AA9 with dioxygen.

Studies have reported the activity of PMOs on cellulose or chitin to be oxidative in nature with dioxygen activation by Cu(I) followed by insertion of one oxygen atom into the substrate (6, 14). We investigated the first step in this proposed reaction sequence by monitoring the reactivity of ascorbate reduced Cu-AA9 with dioxygen by EPR and stopped-flow absorption spectroscopies. Reduced enzyme was mixed with oxygenated buffer in an EPR tube followed by immediate freezing in liquid nitrogen. Within the freezing time of the reaction mixture (<10s), the resting Cu(II)-AA9 was fully regenerated as evaluated by EPR spin integration, consistent with a minimum rate of Cu(I) reoxidation of $>0.15 s^{-1}$ (Fig. S4). This reaction was further performed in a stopped-flow absorption spectrometer, and in agreement with the EPR result, low intensity Cu d-d bands (at 600-700nm) appeared within 10s (Figs. S5A and B).

The reoxidation of Cu(I)-AA9 by O_2 may occur either through inner- or outer-sphere pathways as shown in Scheme 1. In the outer-sphere mechanism (A) O_2 would oxidize Cu(I) and regenerate the resting Cu(II)-AA9 site in a single reaction step, whereas an inner-sphere reaction would involve the formation of a Cu-superoxide

intermediate (B) followed by rapid release of superoxide and regeneration of the resting enzyme state (C).

Scheme 1 Possible reaction pathways for reoxidation of Cu(I)-AA9 by O_2

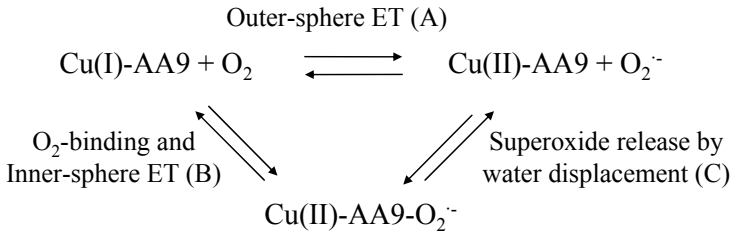

Outer-sphere reoxidation can be evaluated by the Marcus equation (25,26). While no redox potential has been reported for AA9, the redox potential of AA10 enzymes has been reported at ~275mV vs. NHE (15,17). Using this potential, and the potential of the one electron reduction of O_2 to superoxide (-165mV vs. NHE) (27), the outer-sphere electron transfer rate from Cu(I) to O_2 is estimated to be ~$4.5x10^{-4}s^{-1}$ (see SI) which is ~10^3 slower than the experimental rate of Cu(I) reoxidation from the EPR and stopped-flow data. Based on this, the single electron transfer from Cu(I)-AA9 to O_2 likely proceeds via an inner-sphere pathway involving rapid formation of Cu(II)-superoxide, where binding of the $O_2^{\cdot-}$ to the Cu(II) drives the reaction. The fact that only the resting state is observed in the resulting EPR spectrum indicates that the superoxide that has formed is rapidly displaced from the Cu(II) by H_2O. The inner-sphere Cu(II)-superoxide formation followed by water displacement of the superoxide to give the resting Cu(II) state, are computationally evaluated below.

2.3 Experimentally calibrated DFT calculations.

2.3.1 Optimized structures of Cu(I)- and Cu(II)-AA9.

Determination of the Cu(I) and Cu(II)-AA9 coordination environments by Cu K-edge XANES and EXAFS (vide supra) allowed for the optimization of experimentally calibrated DFT structures. As the starting point, a truncated model of the high-resolution (1.50Å) crystal structure of *T.aurantiacus* AA9 (3ZUD) was employed, with a total of six amino acid residues, two providing the three Cu ligands as described above, and two water/hydroxide molecules that are in equatorial and axial orientations with respect to the Cu ion (Fig. S6). The redox state of the Cu ion in the crystal structure is unknown, and the same starting structure was therefore used for optimization of both the oxidized and reduced sites.

Optimization of Cu(I)-AA9 using the B3LYP functional with the 6-311g* basis set on Cu, 6-31g* on the six nearest atoms to Cu, and 3-21g* on the rest, resulted in a three-coordinate Cu(I) site with the two N-His ligands at 1.91Å from the Cu, and the terminal amine-N providing the third ligand at 2.26Å, in an overall T-shaped geometry (Fig. 5A and Table S2). This is in agreement with the experimental XANES and EXAFS results presented above. To further validate the optimized structure, we used this structure to simulate its EXAFS spectrum, and as shown in Fig. S7, top, the simulated EXAFS spectrum is very similar to the experimental Cu(I)-AA9 spectrum. In addition to the first sphere ligands, the equatorial water ligand, which in the starting geometry is at 2.00Å from the Cu(I), moves out of the inner coordination sphere and is found at a 3.11Å distance to the Cu, hydrogen bonded to the conserved Gln-173 residue. Finally, the distances to the axially positioned Tyr-O and water-O (2.92Å and 2.89Å from the Cu in the crystal structure) increased slightly to 3.23Å and 3.32Å, respectively, in the model

(Fig. S8A). A recent computational paper on AA9 enzymes by Kim and co-workers optimized to a four-coordinate Cu(I)-AA9 structure, inconsistent with our experimental data and optimized structure presented here. Possible reasons for this discrepancy are that Kim et al. used a lower resolution crystal structure of AA9 (2YET) as the starting structure and employed the double-zeta 6-31g* basis set on Cu. If we optimize the 3ZUD-based structure used here with the 6-31g* basis set on Cu we also obtain a four-coordinate Cu(I) structure, and additionally if we reoptimize the Cu(I) structure obtained by Kim et al. using the larger triple-zeta 6-311g* basis set on Cu, we obtain a 2+1 coordinate DFT structure, in agreement with the experimental data and our calculations.

For the optimization of the resting Cu(II)-AA9 the starting structure was similar to the starting structure for Cu(I)-AA9 with the only difference being the replacement of the equatorial water by a hydroxide. (The equatorial water-derived ligand is modeled as a hydroxide based on the computational results presented in section 2.3.4.) An optimized structure fully consistent with the experimental data was again obtained, i.e. a four-coordinate tetragonal Cu(II) site with an average Cu-N/O distance of 1.98Å (see Fig. 5B and Table S2). To further validate this structure, the simulated EXAFS spectrum of the optimized Cu(II)-AA9 structure with bound OH^- is found to be in reasonable agreement with the experimental spectrum (Fig. S7, bottom).

2.3.2 O_2-binding to Cu(I)-AA9.

From the fast rate of O_2 reduction by the Cu(I) state that regenerates the resting Cu(II)-AA9 (vide supra), dioxygen appears to undergo the thermodynamically difficult superoxide formation by inner-sphere reduction by the Cu(I) active site. This was

evaluated computationally by adding an O_2 molecule to the optimized Cu(I)-AA9 structure followed by reoptimization (Fig. 6A, Tables S3A and B). (Note that the O_2 in the Cu-O_2 structure displaces the non-coordinating equatorial water which is hydrogen-bonded to Gln-173 in the Cu(I) optimized structure, whereas the axial water moves to a position immediately above the nitrogen N1). In the most stable O_2-bound structure obtained, superoxide binds equatorially to the Cu(II) ion in an end-on fashion. The lowest energy spin state has an S=1 (for MOs see Fig S9), whereas the S=0 open shell singlet (broken symmetry corrected) is ~4.5kcal/mol less stable. It was not possible to stabilize a side-on bound Cu-O_2 structure in the AA9 site. The thermodynamics of O_2 binding to the Cu(I)-AA9 site (from the energies of the Cu-O_2 + H_2O relative to the Cu(I) + O_2) were calculated to be thermoneutral ($\Delta G°$ = -0.5kcal/mol and $\Delta E°$ = -0.7kcal/mol) (Table 2).

In order to evaluate the effect of the included water molecules on the reaction energy and geometric structures, the Cu(II)-superoxide formation was also calculated by optimizing Cu(I) and Cu(II)-O_2-AA9 structures with no waters present (Fig. 6B). This resulted in optimized structures of the reduced and the O_2-bound Cu-AA9 that were very similar to those obtained with the water molecules included (Figs. 6A and B and Tables S3A and B). In terms of binding energy, however, Cu-superoxide formation in the absence of the water molecules is highly favorable ($\Delta E°$ = -14.7kcal/mol) compared to the calculation with water molecules included ($\Delta E°$ = -0.7kcal/mol). However, this favorable binding energy is countered by a decrease in entropy (Table 2) and results in a small decrease in $\Delta G°$ from -0.5kcal/mol with water molecules included to -2.6kcal/mol in the absence of H_2O displacement. Therefore, the slightly favorable free energy of superoxide formation in Cu-AA9 is a property of the protein derived ligation (2xN-His

and 1xN-terminal amine) and not simply a consequence of solvent exposure of the Cu active site.

2.3.3 Comparison of O_2-bound Cu-AA9 to characterized Cu-superoxide model complexes.

Cu-superoxide species have been proposed as reactive intermediates in H-atom abstraction in the non-coupled binuclear Cu enzymes (1, 29,30), although a Cu(II)-superoxide enzyme species has yet to be spectroscopically characterized. Alternatively, a variety of inorganic Cu(II)-superoxide model complexes have been trapped at low temperature (31-35). These include a diaza-cyclooctane supported complex (**1**) (32) (Fig. S10A) and a TMG_3tren supported complex (**2**) (34) (Fig. S10B) both of which have neutral nitrogen ligands to the copper, similar to Cu-AA9. Experimental energies for superoxide formation from reduced **1** (36) and **2** (37) have been reported in acetone (**1)** and DMF (**2**), respectively. In both systems the reaction free energy is close to thermoneutral with **1** being slightly uphill by 1.6 ± 0.2 kcal/mol and **2** being favorable by 1.5 ± 1.7 kcal/mol (Table 2). These experimental values allowed us to evaluate the DFT calculations of reductive O_2 binding by Cu(I)-AA9 presented above.

In order to compare the O_2 binding to Cu-AA9 relative to the model complexes, we optimized reduced and O_2 bound structures of both **1** and **2** (Figs. S10A and B) using the same basis set and functional employed above for Cu-AA9. The $\Delta G°$ for O_2 bonding to reduced **1** is calculated to be +5.3kcal/mol, which is in reasonable agreement with the experimental value of +1.6kcal/mol (Table 2). While the calculated entropy is similar to the experimental value, the O_2 binding energy is slightly less favorable, consistent with

the B3LYP functional that tends toward low bond strengths. Interestingly, the calculated reduced and O_2 bound structures for **1** have very similar geometries compared to the DFT optimized Cu(I)-AA9 and Cu(II)-AA9-superoxide structures (Figs. 6 and S10A and Tables S3A and B). For **2**, the $\Delta G°$ is calculated to be -4.2kcal/mol, again consistent with the experimental value of -1.5kcal/mol. Furthermore, the geometry optimized O_2 bound structure of **2** is very close to the reported crystal structure (Table S3A and B) (34). Interestingly, the entropy is less negative in the calculations compared to experiment, suggesting solvent interaction in the reduced state that would also influence the ΔE calculation. However, since there is no structural information available on reduced **2** this is not included in the model. Overall, the agreement between experiments and calculations of **1** and **2** validates our calculations on the truncated Cu-AA9 enzyme models presented above, supporting the argument for inner-sphere Cu(II)-superoxide formation in the AA9 enzyme.

2.3.4 Release of superoxide in Cu-AA9.

To complete the correspondence between our observed experimental reactivity of reduced Cu-AA9 with dioxygen in the absence of polysaccharide substrate, and the computational results, it is necessary to evaluate the displacement of the superoxide to reform the resting Cu(II)-AA9 site. Displacement of ligands from tetragonal Cu(II) complexes generally involves an associative mechanism. Therefore, an additional water molecule was included at the axial position of the optimized Cu(II)-superoxide enzyme structure (Fig. 6A, right and Fig. S11A) and a linear transit calculation was performed by

displacing the $O_2^{\cdot-}$ moiety in increments of 0.1Å from the Cu(II) with reoptimization of the remaining coordinates (Scheme 2).

Scheme 2 Superoxide release from Cu(II)-AA9. Representations of selected geometry optimized structures with Cu-O1 distances fixed at 2.0, 2.4, 2.6, 2.9, and 3.0Å, respectively. Note that the model structures are rotated 180° with respect to Figure S11.

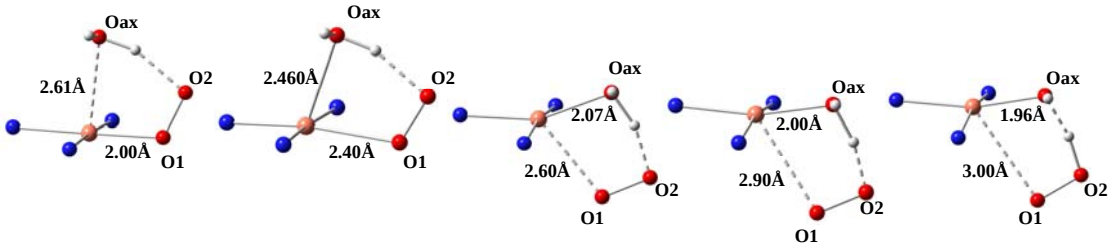

This allowed the axial water molecule to move closer to the Cu(II) and eventually occupy the vacated equatorial position (Scheme 2 and Figs. S11B and C). At a Cu-O_2 distance between 2.9 and 3.0Å a proton from the water shifts to the superoxide, at which point a resting Cu(II)-AA9 structure with an equatorial bound hydroxide ligand is generated. This superoxide release was found to be uphill by 10.3kcal/mol ($\Delta G°$) which is reasonably consistent with the experimentally determined rate of regeneration of the resting Cu(II)-AA9 (>0.15s^{-1}) (vide supra). It is interesting to note, in that context, that in a recent Cu-AA9 crystal structure by Li et al. a superoxide molecule was refined at a distance of ~2.9Å from the Cu-ion (19).

3. Discussion

A detailed description of the active site properties, in solution, of the newly discovered cellulose and chitin degrading *polysaccharide monooxygenases*, AA9-11, is a critical step in understanding how these enzymes perform their O_2 activation utilizing only a single Cu center. From the combination of spectroscopic and computational results presented above, the Cu-AA9 enzyme from *T.aurantiacus* is found to have a four-coordinate tetragonal geometry in its oxidized state, whereas the reduced state of the enzyme has a three coordinate T-shaped structure. The protein derived nitrogen ligands identified by crystallography, N-His1, N-His86 and the terminal amine, coordinate to the Cu(I) and the Cu(II), with protonative loss of a hydroxide ligand upon reduction of the Cu center.

As observed by EPR and stopped-flow absorption spectroscopies, the T-shaped Cu(I) in AA9 undergoes rapid reoxidation when reacted with O_2, with a rate constant of $>0.15 s^{-1}$, consistent with an inner-sphere mechanism where O_2 coordinates to the vacant equatorial position and is concertedly reduced by one electron by the Cu(I). Thus, the binding of the superoxide to the Cu(II) drives the thermodynamically difficult one electron reduction of O_2. This is supported by experimentally calibrated DFT calculations that show O_2 binding as an end-on Cu(II)-superoxide triplet with a slightly favorable free energy.

It is interesting from a structure-function perspective to consider why the single Cu site in PMOs has evolved to incorporate the terminal amine and side chain nitrogen of His1 as ligands. The dual ligation by the His1 residue provides a N-Cu-N angle of ~90°, and by incorporating a third coordinating nitrogen (from His86) at ~180° to N-His1, the

protein-derived coordination sphere allows for the formation of the tetragonal Cu(II) geometry (with addition of an exogenous H_2O ligand as OH^-) and the T-shaped Cu(I) geometry, observed experimentally in this study. Both of these structures are favorable for the Cu ion in the respective oxidation states. This ensures that the Cu ion can cycle between the oxidized and reduced state with relatively limited reorganization of the protein derived ligands thereby promoting rapid reductive O_2 binding. Also, the T-shaped geometry of the Cu(I) provides excellent σ-overlap with the protein-derived ligands, which will raise the energy of the filled antibonding d_{x2-y2} Redox Active Molecular Orbital (RAMO). This, combined with the vacant equatorial coordination position allows for favorable overlap with one of the π*-LUMOs of O_2, resulting in the calculated thermodynamically favorable formation of a Cu-superoxide intermediate.

Finally, the observed (by EPR) regeneration of resting Cu(II)-AA9, in the absence of substrate, indicates rapid release of superoxide. As mentioned in the introduction, the cleavage of cellulose substrate occurs in a controlled manner, inconsistent with random attack by released oxygen species. While the turnover rate for cellulose cleavage has yet to be determined in AA9 enzymes, it is likely that this is a relatively slow process based on the long time scale employed in activity assays (6, 7, 11, 14,18). Therefore the observed rapid superoxide release must be limited when substrate is bound to the enzyme. As evaluated by the DFT calculations, the tetragonal Cu-superoxide allows for a water molecule to enter the axial coordinate position which would result in associative displacement of the superoxide with a relatively low barrier (10.3kcal/mol). Substrate binding to the enzyme surface (Fig. 1, left) may block the axial position which would then lead to stabilization of the Cu-superoxide intermediate, and prevent its decay to the

resting form of the enzyme. It is interesting to note that in a recently published study by Isaksen et al. (38), hydrogen peroxide formation, by a Cu-AA9 enzyme with different reductants and O_2, was detected only in the absence of substrate or with substrates that were not subject to AA9 activity. If the superoxide is indeed stabilized by the substrate, it may be able to directly attack the polysaccharide, or it may be further reduced to a more reactive species by either small molecules or *cellobiose dehydrogenase* (a known AA9 reducing co-factor) (7,13,39). This awaits further experimental investigation.

In summary, we have determined the coordination geometries for Cu(I) and Cu(II)-AA9 in solution, and found that the enzyme active site structure is well configured for rapid inner-sphere reductive activation of O_2 by Cu(II)-superoxide formation. This is an important step towards elucidating the mechanism by which this new class of mono-nuclear Cu oxygenases functions to activate the inert O_2 molecule by one electron reduction for subsequent degradation of polysaccharides.

Materials and Methods. For details, see SI Materials and Methods. AA9 from *T.aurantiacus* was expressed and purify in accordance with previously published protocols (34). The AA9 enzyme was purified in the Apo-form and loaded with $Cu(II)(NO_3)_2$ to a final Cu concentration of 90-95% compared to the enzyme concentration. All experiments were conducted in 25mM MES buffer, pH 6 unless otherwise stated. DFT calculations were performed with the Gaussian 09 software package (for full reference, see SI).

Acknowledgements. Research reported in this publication was supported by the National Institute of Diabetes and Digestive and Kidney Diseases of the National Institutes of Health under award R01DK031450 (to E.I.S.) and NIH P41GM103393 (to K.O.H). C.H.K. acknowledges a John Stauffer Stanford Graduate Fellowship. Use of the Stanford Synchrotron Radiation Lightsource, SLAC National Accelerator Laboratory, is supported by the U.S. Department of Energy, Office of Science, Office of Basic Energy Sciences under Contract No. DE-AC02-76SF00515. The SSRL Structural Molecular Biology Program is supported by the DOE Office of Biological and Environmental Research, and by the National Institutes of Health, National Institute of General Medical Sciences (including P41GM103393). The contents of this publication are solely the responsibility of the authors and do not necessarily represent the official views of NIGMSor NIH.

References

1. Solomon EI, *et al.* (2011) Copper dioxygen (bio) inorganic chemistry. *Faraday Discussions* 148:11-39.

2. Solomon EI, Augustine AJ, & Yoon J (2008) O(2) Reduction to H(2)O by the multicopper oxidases. *Dalton Transactions* (30):3921-3932.

3. Mano N, *et al.* (2003) Oxygen is electroreduced to water on a "wired" enzyme electrode at a lesser overpotential than on platinum. *Journal of the American Chemical Society* 125(50):15290-15291.

4. Ginsbach JW, *et al.* (2012) Structure/function correlations among coupled binuclear copper proteins through spectroscopic and reactivity studies of NspF. *Proceedings of the National Academy of Sciences of the United States of America* 109(27):10793-10797.

5. Klinman JP (2006) The copper-enzyme family of dopamine beta-monooxygenase and peptidylglycine alpha-hydroxylating monooxygenase: Resolving the chemical pathway for substrate hydroxylation. *Journal of Biological Chemistry* 281(6):3013-3016.

6. Vaaje-Kolstad G, *et al.* (2010) An Oxidative Enzyme Boosting the Enzymatic Conversion of Recalcitrant Polysaccharides. *Science* 330(6001):219-222.

7. Quinlan RJ, *et al.* (2011) Insights into the oxidative degradation of cellulose by a copper metalloenzyme that exploits biomass components. *Proceedings of the National Academy of Sciences of the United States of America* 108(37):15079-15084.

8. Glyn R Hemsworth BH, Gideon J Davies, Paul H Walton (2014) Discovery and characterization of a new family of lytic polysaccharide monooxygenases. *Nature Chemical Biology* 10:122-126.

9. Levasseur A, Drula E, Lombard V, Coutinho PM, & Henrissat B (2013) Expansion of the enzymatic repertoire of the CAZy database to integrate auxiliary redox enzymes. *Biotechnology for Biofuels* 6.

10. Hemsworth GR, Davies GJ, & Walton PH (2013) Recent insights into copper-containing lytic polysaccharide mono-oxygenases. *Current Opinion in Structural Biology* 23(5):660-668.

11. Harris PV, *et al.* (2010) Stimulation of Lignocellulosic Biomass Hydrolysis by Proteins of Glycoside Hydrolase Family 61: Structure and Function of a Large, Enigmatic Family. *Biochemistry* 49(15):3305-3316.

12. Forsberg Z*, et al.* (2011) Cleavage of cellulose by a CBM33 protein. *Protein Science* 20(9):1479-1483.

13. Phillips CM, Beeson WT, Cate JH, & Marletta MA (2011) Cellobiose Dehydrogenase and a Copper-Dependent Polysaccharide Monooxygenase Potentiate Cellulose Degradation by Neurospora crassa. *Acs Chemical Biology* 6(12):1399-1406.

14. Beeson WT, Phillips CM, Cate JHD, & Marletta MA (2012) Oxidative Cleavage of Cellulose by Fungal Copper-Dependent Polysaccharide Monooxygenases. *Journal of the American Chemical Society* 134(2):890-892.

15. Aachmann FL, Sorlie M, Skjak-Braek G, Eijsink VGH, & Vaaje-Kolstad G (2012) NMR structure of a lytic polysaccharide monooxygenase provides insight into copper binding, protein dynamics, and substrate interactions. *Proceedings of the National Academy of Sciences of the United States of America* 109(46):18779-18784.

16. Vu VV, Beeson WT, Phillips CM, Cate JHD, & Marletta MA (2014) Determinants of Regioselective Hydroxylation in the Fungal Polysaccharide Monooxygenases. *Journal of the American Chemical Society* 136(2):562-565.

17. Hemsworth GR*, et al.* (2013) The Copper Active Site of CBM33 Polysaccharide Oxygenases. *Journal of the American Chemical Society* 135(16):6069-6077.

18. Wu M*, et al.* (2013) Crystal Structure and Computational Characterization of the Lytic Polysaccharide Monooxygenase GH61D from the Basidiomycota Fungus Phanerochaete chrysosporium. *Journal of Biological Chemistry* 288(18):12828-12839.

19. Li X, Beeson WT, Phillips CM, Marletta MA, & Cate JHD (2012) Structural Basis for Substrate Targeting and Catalysis by Fungal Polysaccharide Monooxygenases. *Structure* 20(6):1051-1061.

20. Macedo S*, et al.* (2009) Can soaked-in scavengers protect metalloprotein active sites from reduction during data collection? *Journal of Synchrotron Radiation* 16:191-204.

21. Smith TA, Penner-Hahn JE, Hodgson KO, Berding MA, & Doniach S (1984) Polarized Cu K-Edge studies. *EXAFS and Near Edge Structure III. Proceedings of an International Conference*:58-60.

22. Kau LS, Spirasolomon DJ, Pennerhahn JE, Hodgson KO, & Solomon EI (1987) X-ray absorption edge determination of the oxidation state and coordination number of copper- application to the type-3 site in Rhus verrnicifera laccase and

its reaction with oxygen. *Journal of the American Chemical Society* 109(21):6433-6442.

23. Balasubramanian R*, et al.* (2010) Oxidation of methane by a biological dicopper centre. *Nature* 465(7294):115-199

24. Smith SM*, et al.* (2011) Crystal Structure and Characterization of Particulate Methane Monooxygenase from Methylocystis species Strain M. *Biochemistry* 50(47):10231-10240.

25. Marcus RA (1964) Chemical electron-transfer theory and electron-transfer theory. *Annual Review of Physical Chemistry* 15:155-&.

26. Marcus RA (1993) Electron-transfer reactions in chemistry- theory and experiment (Nobel Lecture). *Angewandte Chemie-International Edition in English* 32(8):1111-1121.

27. Wood PM (1988) The potential diagram fro oxygen at pH-7. *Biochemical Journal* 253(1):287-289.

28. Kim S, Stahlberg J, Sandgren M, Paton RS, & Beckham GT (2014) Quantum mechanical calculations suggest that lytic polysaccharide monooxygenases use a copper-oxyl, oxygen-rebound mechanism. *Proceedings of the National Academy of Sciences of the United States of America* 111(1):149-154.

29. Prigge ST, Eipper BA, Mains RE, & Amzel LM (2004) Dioxygen binds end-on to mononuclear copper in a precatalytic enzyme complex. *Science* 304(5672):864-867.

30. Evans JP, Ahn K, & Klinman JP (2003) Evidence that dioxygen and substrate activation are tightly coupled in Dopamine-*β*-Monooxygenase. *Journal of Biological Chemistry* 278(50):49691-49698.

31. Chen P, Root DE, Campochiaro C, Fujisawa K, & Solomon EI (2003) Spectroscopic and electronic structure studies of the diamagnetic side-on Cu-II-superoxo complex Cu(O-2) HB(3-R-5-(i)Prpz)(3) : Antiferromagnetic coupling versus covalent delocalization. *Journal of the American Chemical Society* 125(2):466-474.

32. Kunishita A*, et al.* (2009) Mononuclear Copper(II)-Superoxo Complexes that Mimic the Structure and Reactivity of the Active Centers of PHM and DβM. *Journal of the American Chemical Society* 131(8):2788-2789

33. Ginsbach JW, Peterson RL, Cowley RE, Karlin KD, & Solomon EI (2013) Correlation of the Electronic and Geometric Structures in Mononuclear Copper(II) Superoxide Complexes. *Inorganic Chemistry* 52(22):12872-12874.

34. Wuertele C*, et al.* (2006) Crystallographic characterization of a synthetic 1 : 1 end-on copper dioxygen adduct complex. *Angewandte Chemie-International Edition* 45(23):3867-3869.

35. Donoghue PJ, Gupta AK, Boyce DW, Cramer CJ, & Tolman WB (2010) An Anionic, Tetragonal Copper(II) Superoxide Complex. *Journal of the American Chemical Society* 132(45):15869-15871.

36. Kunishita A*, et al.* (2012) Active Site Models for the Cu-A Site of Peptidylglycine alpha-Hydroxylating Monooxygenase and Dopamine beta-Monooxygenase. *Inorganic Chemistry* 51(17):9465-9480.

37. Lanci MP*, et al.* (2007) Isotopic probing of molecular oxygen activation at copper(I) sites. *Journal of the American Chemical Society* 129(47):14697-14709.

38. Isaksen *et al.* (2014) A C4-oxidizing Lytic Polysaccharide Monooxygenase Cleaving Both Cellulose and Cello-oligosaccharides. The journal of biological chemistry. 289: 2632-2642

39. Bey M*, et al.* (2013) Cello-Oligosaccharide Oxidation Reveals Differences between Two Lytic Polysaccharide Monooxygenases (Family GH61) from Podospora anserina. *Applied and Environmental Microbiology* 79(2):488-496.

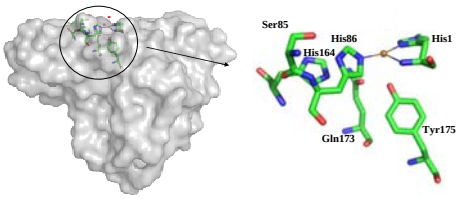

Figure 1 AA9 from *T.aurentiacus* (modified from pdb: 3ZUD). Surface view (left) and active site (right) highlighting six selected residues surrounding the Cu ion (gold sphere).

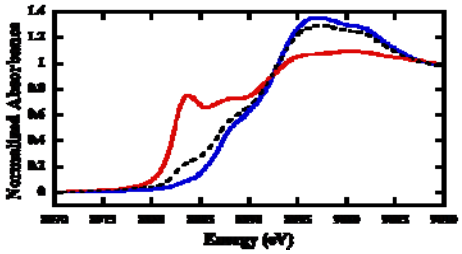

Figure 2 Normalized Cu K-edge XANES spectra of Cu loaded AA9, Cu(II)- first short, fast scan (blue) , Cu(II)-average of first scans from four fresh spots (black), and Cu(I) (red).

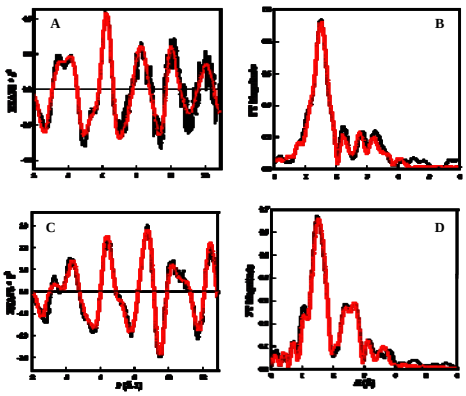

Figure 3 Cu K-edge EXAFS data (A) and non-phase-shift-corrected Fourier transform (B) of Cu(II)-AA9. Cu K-edge EXAFS data (C) and non-phase-shift-corrected Fourier transform (D) of Cu(I)-AA9. Phase shifts in the first shells are ~0.4 Å. Data (black), Fits (red).

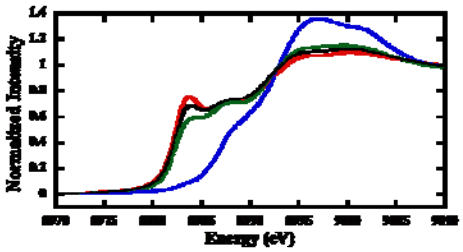

Figure 4 Normalized Cu K-edge XANES spectra of ~75% cryo-reduced Cu-AA9, first scan (green) and ~90% cryo-reduced Cu-AA9 (black). Spectra of Cu(I) (red scan) and Cu(II)-AA9 (blue scan) from Fig. 2.

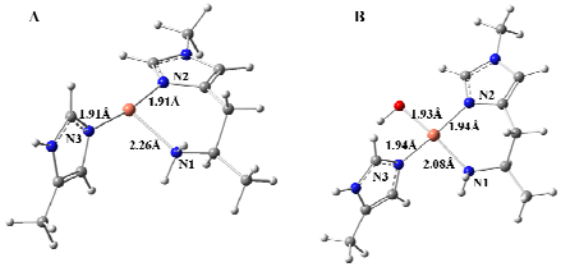

Figure 5 DFT structures of Cu-AA9. Optimized structure of Cu(I)-AA9 (A), and optimized structure of Cu(II)-AA9 with OH^- as equatorial ligand (B). For complete structures, see Fig. S8A and B.

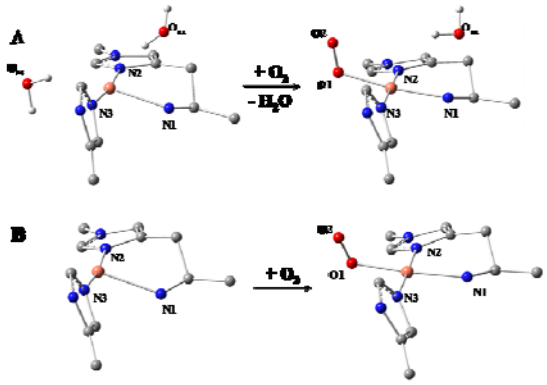

Figure 6 Representations of DFT optimized structures of reduced and O_2-bound Cu-AA9. Cu-AA9 reduced with water molecules included (A, left) and O_2-bound with equatorial water displaced by O_2 (A, right). Cu-AA9 reduced with water molecules removed (B, left) and O_2-bound (B, right). Hydrogen atoms are omitted for clarity, except for water molecules in (A)**.**

Table 1A EXAFS Least-Squares Fitting Results for $k = 2-12.8$ Å^{-1} for Cu(II)-AA9

Coord no./Path	R (Å)[a]	σ^2(Å^2)[b]	ΔE_0 (eV)	F[c]
4 Cu-N/O	1.98	500	-8.59	0.28
5 Cu-C	2.94	761		
8 Cu-N-C	3.13	801		
4 Cu-N/C	3.87	965		
16 Cu-N-C	4.11	965		
8 Cu-N-C	4.73	603		

Table 1B EXAFS Least-Squares Fitting Results for $k = 2-12.8$ Å^{-1} for Cu(I)-AA9

Coord no./Path	R (Å)[a]	σ^2(Å^2)[b]	ΔE_0 (eV)	F[c]
2 Cu-N/O	1.90	308	-9.75	0.06
1 Cu-N/O	2.25	665		
4 Cu-C	2.92	275		
8 Cu-N-C	3.06	582		
4 Cu-N/C	3.90	932		
16 Cu-N-C	4.07	864		

[a]The estimated standard deviation in R for each fit is ±0.02 Å. [b]The σ^2 values are multiplied by 10^5. [c]The error, F, is given by $\sum[(\chi_{obsd} - \chi_{calcd})^2 k^6]/\sum[(\chi_{obsd})^2 k^6]$. The error in coordination number is 25%, and that in the identity of the scatterer Z is ±1.

Table 2 DFT calculated thermodynamic values for O_2 binding to Cu(I)-AA9. DFT calculated and experimentally determined thermodynamic values for O_2 binding to Cu(I)-model complexes **1** and **2**

	ΔE (kcal/mol)	ΔH (kcal/mol)	ΔS (cal/mol)	ΔG (kcal/mol)
O_2-Cu(II)-AA9	-0.7	-2.5	-6.7	-0.5
O_2-Cu(II)-AA9 no H_2O	-14.7	-13.7	-37.4	-2.6
O_2-**1 (**ref 36) (experimental)	-	-9.1±0.3	-35.8±0.7	1.6±0.2
O_2-**1** (calculated)	-6.1	-4.7	-33.7	5.3
O_2-**2** (ref 37) (experimental)	-	-8.4±0.8	-23.0±3	-1.5±1.7
O_2-**2** (calculated)	-17.9	-15.7	-38.7	-4.2